

# Effects of strut geometry and pore fraction on creep properties of cellular materials

Yuttanant Boonyongmaneerat<sup>a</sup>, David C. Dunand<sup>b,\*</sup>

<sup>a</sup> *Metallurgy and Materials Science Research Institute, Chulalongkorn University, Bangkok 10330, Thailand*

<sup>b</sup> *Department of Materials Science and Engineering, Northwestern University, Evanston, IL 60208, USA*

Received 6 October 2008; received in revised form 11 November 2008; accepted 11 November 2008

Available online 2 January 2009

## Abstract

A set of analytical models based on engineering beam analysis is developed to predict creep behavior of cellular materials over a broad range of relative density. Model predictions, which take into account the presence of mass at strut nodes and consider different possible deformation mechanisms and foam architectures, are compared to experimental creep results for a replicated nickel-base foam and a reticulated aluminum foam. As porosity decreases, the controlling creep mechanism in the foams changes from strut bending, to strut shearing, and ultimately to strut compression.

© 2008 Acta Materialia Inc. Published by Elsevier Ltd. All rights reserved.

*Keywords:* Creep; Foams; Porous materials; Sponges; Metallic foams

## 1. Introduction

The creep deformation of cellular materials (or foams) is important for load-bearing applications at high homologous temperatures. For creep-resistant applications, metallic foams are particularly interesting, since they have higher creep resistance and oxidation resistance than polymer foams and higher toughness than ceramic foams. Most metallic foams studied to date are based on aluminum produced by melt foaming [1–3]. Foam creep models have thus focused mostly on low-density reticulated foams with or without cell walls [4–6]. Unlike aluminum foams, high-melting metal foams cannot easily be produced by gas injection or generation in the melt, due to their high liquidus temperature and reactivity. Rather, replication methods have been used for various high-melting alloys such as nickel-, iron-, and titanium-base foams [7–12] as well as for aluminum with higher relative densities than reticulated foams [13–15]: liquid metal is poured, or powders are densified, in the space present within a partially densified preform of space-holder

powders (usually a salt or oxide) which are subsequently removed to create porosity. Replicated foams thus show open pores but they exhibit struts which are much less uniform in cross-sectional area than those in reticulated foams: they are thick at their nodes and become progressively thinner toward their mid-points, reflecting the shape of the empty space between the contacting space-holder particles. Thus, replicated metal foams, with typically 30–85% open porosity, have an architecture intermediate between reticulated foams (with struts of uniform diameter connected by nodes, and with open porosities above ~85%) and porous metals (consisting of distinct pores within a continuous matrix, with fully or partially closed porosities under ~30%).

To date, research on creep of metallic foams has focused on reticulated Al and Ni foams with porosity over ~85% for which models have been developed considering the compressive or bending deformation of struts with uniform cross-sections. Extending these models to higher relative density for replicated foams may be inadequate, since the struts of these foams have non-uniform sections and low aspect ratios, which may lead to combined compression and bending deformation mechanisms or even new mechanisms such as shearing.

\* Corresponding author. Tel.: +1 847 491 5370.

E-mail address: [dunand@northwestern.edu](mailto:dunand@northwestern.edu) (D.C. Dunand).

In the present work, we address this issue by developing a series of analytical models to predict creep behavior of metallic foams over a broad range of porosity values and for various strut geometries. This is achieved by modifying existing creep models for high-porosity reticulated foams which are based on bending [1,4] or compression [16] of uniform struts. Predictions of the modified models, which explicitly consider the presence of mass at nodes as well as a range of deformation mechanisms and foam architectures, are compared to experimental foam creep results for a replicated nickel-base foam reported here and an aluminum reticulated foam reported previously in the literature [4].

## 2. Creep models

### 2.1. Existing creep models

#### 2.1.1. Beam analysis models

For a monolithic material, the secondary creep behavior may be expressed by the power-law creep equation as

$$\dot{\epsilon}_s = A\sigma_s^n \exp\left(\frac{-Q}{RT}\right) = K\sigma_s^n \quad (1)$$

where  $\dot{\epsilon}_s$  is the uniaxial strain rate,  $A$  the creep constant,  $\sigma_s$  the uniaxial stress,  $n$  the stress exponent,  $Q$  the creep activation energy,  $R$  the gas constant, and  $T$  the temperature. The creep constant and the Arrhenius term in Eq. (1) are often combined into a single parameter  $K = A \exp(-Q/RT)$  for simplicity. For foams, the uniaxial stress and strains are usually compressive.

Gibson and Ashby [1,4] developed a simple expression for uniaxial creep of an open-cell reticulated foam:

$$\dot{\epsilon} = \frac{0.6}{n+2} \left(\frac{1.7(2n+1)}{n}\right)^n \rho^{-(3n+1)/2} K\sigma^n \quad (2)$$

where  $\dot{\epsilon}$  and  $\rho$  are the foam strain rate and relative density, respectively. This expression is valid for open-cell foams

whose repeat unit (which after mirroring produces a unit cell) consists of one node connecting three struts of uniform cross-section (Fig. 1), and it assumes that deformation of the structure is controlled solely by the creep bending of the strut perpendicular to the applied stress, with the two other struts parallel to the stress assumed to be rigid. The expression is found to correspond generally well with the creep behavior of reticulated Al foams observed experimentally [4]. We call this model (Eq. (2)) the Gibson–Ashby bending (GA-b) model.

Hodge and Dunand [16] developed an alternative expression for the creep of foams, based on a different reticulated architecture. In their model, a node connects six struts (Fig. 2), so that struts perpendicular to the applied stress are prevented from bending. Deformation is assumed to be solely due to the uniaxial compressive deformation of struts parallel to the applied stress and the foam strain rate is given by

$$\dot{\epsilon} = \left(\frac{\rho}{3}\right)^{-n} K\sigma^n \quad (3)$$

Eq. (3) generally predicts lower strain rate than Eq. (2) for a given relative density and stress exponent, especially at low relative densities [16]. The relative density below which the foam strain rate in Eq. (3) is lower than that in Eq. (2) is  $\sim 0.3$  for  $n = 1$ , increasing for higher  $n$  values ( $\sim 0.7$  for  $n = 5$ ). We call this model the Hodge–Dunand compression (HD-c) model.

Both GA-b and HD-c models were developed using the engineering beam analysis approach, which considers foam architectures coupled with some relevant deformation mechanisms. Their use is however limited to foams with low relative densities ( $\sim 0.2$  and below), partly due to a series of simplifications made in deriving these equations which prevent the models to be justifiable at higher foam relative density. In particular, in the GA-b model, it is assumed that the uniaxial force  $F$ , strain rate, and relative

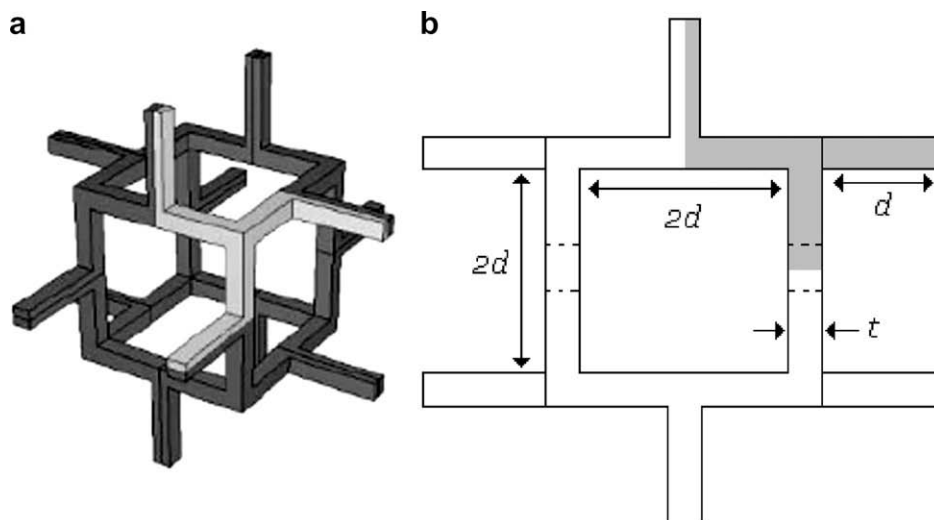


Fig. 1. Gibson–Ashby model ( $\rho = 0.04$ ) shown (a) in three dimensions for unit cell (dark) and repeat unit (light) [21] and (b) in projection with geometric parameters  $d$  and  $t$ .

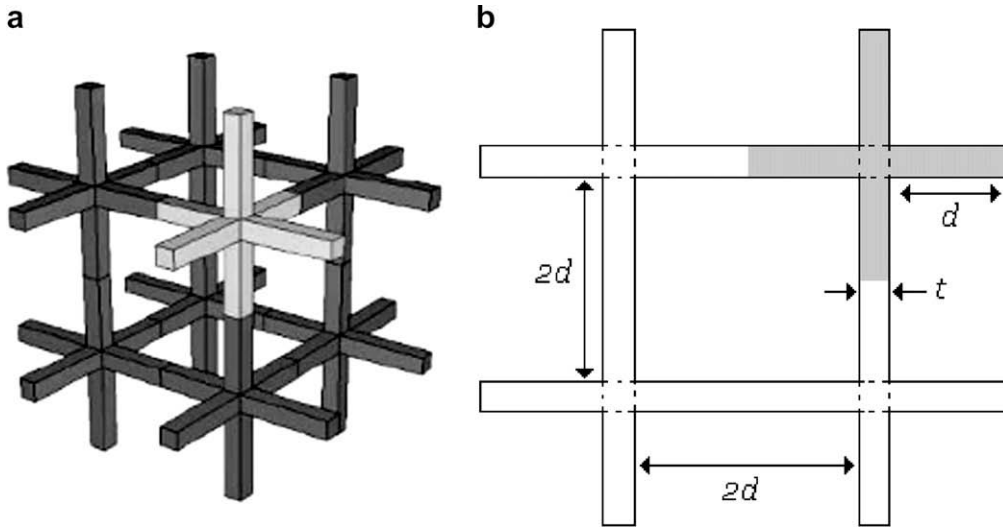


Fig. 2. Hodge–Dunand model ( $\rho = 0.05$ ) shown (a) in three dimensions for extended unit cell (dark) and unit cell (light) [21] and (b) in projection with geometric parameters  $d$  and  $t$ .

density are proportional to strut dimensions according to  $F \propto \sigma \cdot l^2$ ,  $\dot{\epsilon} \propto \delta/l$ , and  $\rho \propto (t/l)^2$ , where  $\delta$  is the rate of deflection of struts perpendicular to the uniaxial force, and  $t$  and  $l$  are, respectively, the thickness and length of foam struts. However, these approximations are accurate only when struts are fairly slender at low relative densities. In the HD-b model, it is assumed that the mass at nodes is small compared to that of the struts, so that the assumption that one third, rather than the totality, of the node volume is load-bearing is acceptable. This approximation becomes less and less valid as the relative density increases, because the node mass increases more rapidly than the strut mass.

### 2.1.2. Composite analysis models

By utilizing the mean-field theory and simplifying the variational estimates for non-linear composite deformation, Mueller et al. developed an analytical expression for the uniaxial steady state creep rate of metallic foams as [17]:

$$\dot{\epsilon} = F_E^{-(1+n)/2} \rho^{-(n-1)/2} K \sigma^n \quad (4)$$

where  $F_E$  is the ratio of the Young's modulus of foams and monolithic materials, which may be expressed as  $F_E = A_E \rho^\alpha$ , where  $A_E$  is a fitting parameter typically close to unity. For open-cell foams with low to intermediate relative density (less than  $\sim 0.5$ ), the exponent is  $\alpha \approx 2$ . At higher relative densities, it was experimentally determined as  $\alpha \approx 1.2$  [18]. For sintered powder-based materials with relative density above  $\sim 0.8$ , the value of  $\alpha$  may be as low as 0.3 [19]. The strain rate relationship obtained by Eq. (4) produces trends similar to those of the GA-b model in the low-density range [17]. This mean-field (MF) model will be discussed in relation to other models based on beam analysis in later sections.

## 2.2. Strut bending models based on the GA-type cell

In this section, we develop analytical expressions to refine the GA-b model (Eq. (2) and Fig. 1) by considering explicitly the presence of rigid nodes. We also consider variants of the model where shearing of horizontal struts replaces bending, and where compression of vertical struts contributes to the overall deformation.

### 2.2.1. Modified bending mechanism

We follow here the same derivation presented in Ref. [4] with the same unit cell foam geometry of the original GA-b model but replace the strut total length  $l$  in the original derivation with the value  $d - t/2$  (where  $d$  and  $t$  are, respectively, the strut half length and its thickness, as shown in Fig. 1), thus taking explicitly into account the non-zero width of the nodes, given by the strut thickness  $t$ . The resulting equation for  $\dot{\delta}$ , the rate of deflection for struts perpendicular to the uniaxial load, is then

$$\dot{\delta} = \frac{\dot{\epsilon}_s}{n+2} \cdot \frac{(d-t/2)^2}{t} \cdot \left(\frac{2n+1}{n}\right)^n \cdot \left(\frac{F(d-t/2)}{\sigma_s \cdot t^3}\right)^n \quad (5)$$

Thus, it is assumed that nodes remain rigid while the four horizontal strut sections with length  $d - t/2$  of the GA cell are deforming by creep bending, as illustrated in Fig. 3a. The foam remote strain rate and stress are related to the displacement rate and load through the dimensional arguments:

$$\dot{\epsilon} = k_1 \dot{\delta} / (d + t/2) \quad (6)$$

$$F = k_2 \sigma (d + t/2)^2 \quad (7)$$

where  $k_1$  and  $k_2$  are dimensionless constants. These equations are again similar to those used in Ref. [4], except that the strut length  $l$  is replaced with  $d - t/2$ . Furthermore, the third assumption in the GA-b model concerning the relative density ( $\rho \propto (t/l)^2$ ) is replaced with a more complex

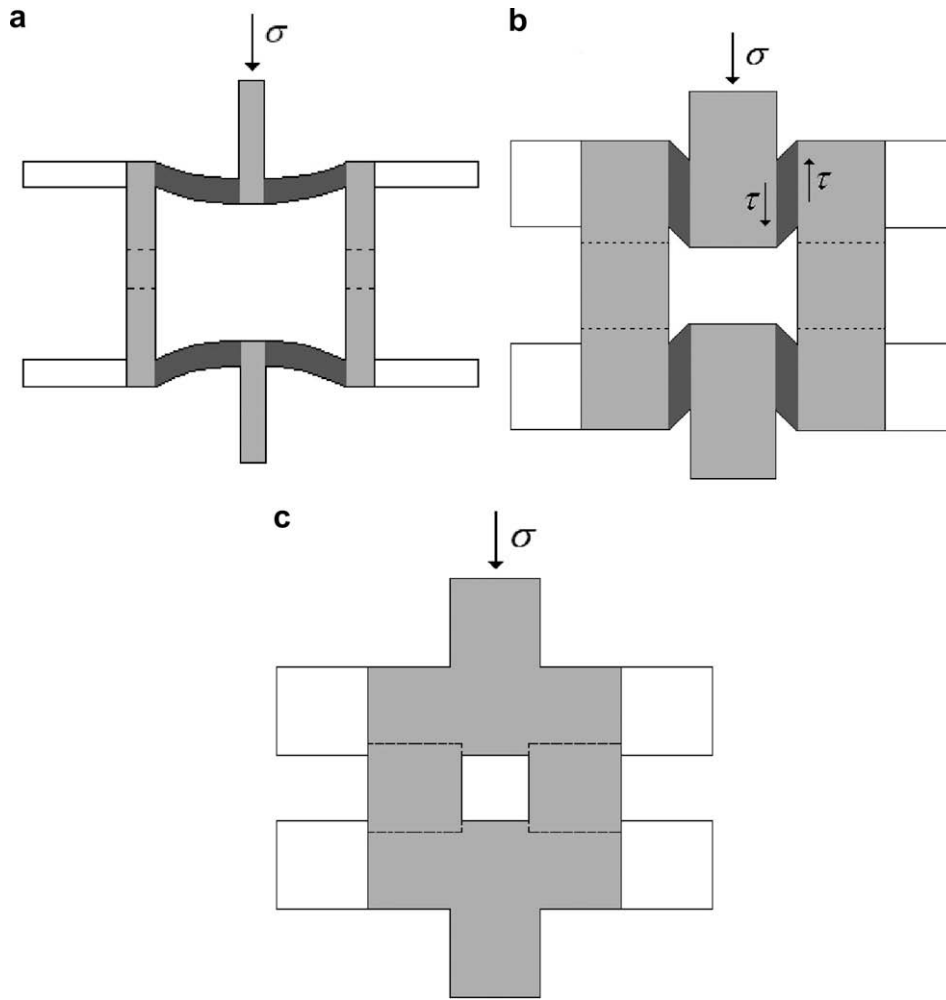


Fig. 3. Gibson–Ashby model shown in projection (a) for low relative density ( $\rho = 0.04$ ); (b) for intermediate relative density ( $\rho = 0.30$ ); (c) for high relative density ( $\rho = 0.50$ ). The possible deformation mechanism of this model is bending (GA-b') or bending/compression (GA-bc) in (a), shearing (GA-s) or shearing/compression (GA-sc) in (b), and compression (GA-c) in (c). Volumes undergoing deformation are shaded dark grey for bending or shearing, and light grey for compression.

equation (Eq. (A1) in Appendix A) relating relative density with the strut length  $2d$  and width  $t$ . This equation can further be simplified into Eq. (A2), which defines the relative density of the foam as a function of a single parameter, the strut aspect ratio  $a = 2d/t$ . Introducing Eqs. (6), (7), and (A2) into Eq. (5), we obtain

$$\dot{\epsilon} = \frac{k_1 k_2^n}{n+2} \left( \frac{(2n+1)}{n} \right)^n \cdot \left[ \left( \frac{a-1}{2} \right)^{2+n} \cdot \left( \frac{a+1}{2} \right)^{2n-1} \right] \cdot \dot{\epsilon}_s \left( \frac{\sigma}{\sigma_s} \right)^n \quad (8)$$

The values of the constants  $k_1$  and  $k_2$  (determined in Appendix B as  $k_1 = 3.1$  and  $k_2 = 9.3$  over a range of relative density of 0–0.15) are introduced in Eq. (8) to give

$$\dot{\epsilon} = \frac{3.1}{n+2} \left( \frac{9.3 \cdot (2n+1)}{n} \right)^n \cdot \left[ \left( \frac{a-1}{2} \right)^{2+n} \cdot \left( \frac{a+1}{2} \right)^{2n-1} \right] \cdot K \sigma^n \quad (9)$$

This equation is labeled “modified Gibson–Ashby bending” (GA-b') in the following, as it is a modified version

of Eq. (2) assuming bending of horizontal struts, but taking into account explicitly the node size.

### 2.2.2. Shearing mechanism

In the GA-type models, as the strut aspect ratio decreases with increasing foam relative density, a possible alternative deformation mechanism to bending for the horizontal strut is shearing. As illustrated in Fig. 3b, any pair of adjacent vertical rigid struts translating vertically towards each other along the direction of the applied stress can result in shearing of the horizontal strut connecting them, rather than bending. To determine the strain rate for foams experiencing such deformation mechanism, we first consider the relationship between shear strain rate  $\dot{\gamma}$  and shear stress  $\tau$ :

$$\dot{\gamma} = K' \tau^n = 3^{(n-1)/2} K \tau^n \quad (10)$$

where  $K'$  is a constant and the pre-factor  $3^{(n-1)/2}$  is derived based on Eq. (1) and the relationships between tensile and shear strain rates and stresses [20]. Based on foam geometry, Eq. (10) may also be written as

$$\frac{\dot{\delta}}{(d-t/2)} = 3^{(n-1)/2} K \cdot \left(\frac{F/2}{t^2}\right)^n \quad (11)$$

Finally, we assume that  $\dot{\delta}$  and  $F$  relate, respectively, to  $\dot{\epsilon}$  and  $\sigma$  through the relationships given in Eqs. (6) and (7). After introducing these equations in Eq. (11), the strain rate for the GA-s model deforming by strut shearing (Fig. 3b), rather than strut bending Fig. 3a), is given as

$$\dot{\epsilon} = 1.8 \cdot 8.1^n \left[ \left(\frac{a-1}{2}\right) \cdot \left(\frac{a+1}{2}\right)^{2n-1} \right] \cdot K \sigma^n \quad (12)$$

This equation is labeled “Gibson–Ashby shear” (GA-s) in the following.

### 2.2.3. Combined bending and compression mechanisms

In addition to bending of horizontal struts as discussed in Section 2.2.1, the assumption that vertical foam struts are rigid can be relaxed. Then, the contribution of strut bending (Eq. (9)) and strut compression, which are independent of each other, can be added. First, we develop an expression for the compressive strain rate of vertical struts, which is given by an equation similar to Eq. (3), modified to take into account more precisely the ratio of volume of vertical struts and associated nodes deforming under compressive load ( $V_c$ ) to the total volume of foam material ( $V_t$ ), for the case of the unit cell of GA model (Fig. 1):

$$\frac{V_c}{V_t} = \frac{\frac{3}{2}dt^2 + \frac{3}{4}t^3}{\frac{9}{2}dt^2 + t^3} = \frac{3a+3}{9a+4} \quad (13)$$

where  $V_c$  is calculated as the sum of the two vertical strut volumes and half the volume of the two corresponding nodes in the repeat unit of Fig. 1. This ratio is assumed to be 1/3 in the original HD-c model in Eq. (3). Since the area under compression is the total area of the unit cell divided by  $\rho V_c/V_t$ , the stress exerted on the vertical foam struts ( $\sigma_v$ ) is

$$\sigma_v = \frac{\sigma}{\left(\frac{3a+3}{9a+4}\right)\rho} \quad (14)$$

Introducing this stress into Eq. (1), the resulting strain rate for foam with a GA unit cell deforming solely by creep compression of vertical struts is

$$\dot{\epsilon} = \left(\frac{3a+3}{9a+4} \cdot \rho\right)^{-n} K \sigma^n \quad (15)$$

Combining the above expression with the strain-rate contribution from the bending mechanism (Eq. (9)) gives

$$\dot{\epsilon} = \left[ \frac{3.1}{n+2} \left(\frac{9.3(2n+1)}{n}\right)^n \cdot \left[\left(\frac{a-1}{2}\right)^{2+n} \cdot \left(\frac{a+1}{2}\right)^{2n-1}\right] + \left(\frac{3a+3}{9a+4} \cdot \rho\right)^{-n} \right] \cdot K \sigma^n \quad (16)$$

This equation is labeled “Gibson–Ashby bending/compression” (GA-bc) in the following.

### 2.2.4. Combined shearing and compression mechanisms

Shearing of horizontal struts in GA-s model may be coupled with compression of vertical struts of foams. The

strain rate of such a system, experiencing independently shearing and compressive deformations, is found by combining Eqs. (12) and (15):

$$\dot{\epsilon} = \left[ 1.8 \cdot 8.1^n \left[ \left(\frac{a-1}{2}\right) \cdot \left(\frac{a+1}{2}\right)^{2n-1} \right] + \left(\frac{3a+3}{9a+4} \cdot \rho\right)^{-n} \right] K \sigma^n \quad (17)$$

This equation is labeled “Gibson–Ashby shearing/compression” (GA-sc) in the following.

## 2.3. Strut compression models based on the HD-type cell

In this section, we develop analytical expressions to refine the HD-c model (Eq. (3) and Fig. 2) by considering more accurately the contribution of creeping nodes and also by examining the effect of mass concentration at nodes, both of which become more important when the foam relative density increases.

### 2.3.1. Compression mechanism

The HD-c model (Eq. (3)) assumes that one third of the material in the foam deforms under compression. This corresponds to one third of the struts (the vertical struts parallel to the applied stress) and one third of the node volume. While the strut volume is exact, the node volume is underestimated, because the whole node (rather than only one third of the node) is subjected to the compressive stress and creeping. Then, the foam strain rate in Eq. (3) is underestimated, and the error increases with increasing relative density. Similar to Section 2.2.3, we examine the ratio of the volume of vertical struts and node under compressive load ( $V_c$ ) to the total volume of solid ( $V_t$ ) in the HD unit cell (Fig. 2):

$$\frac{V_c}{V_t} = \frac{2dt^2 + t^3}{6dt^2 + t^3} = \frac{a+1}{3a+1} \quad (18)$$

As before, the stress on the vertical struts and node is given by  $\sigma_v = \sigma/\rho(V_c/V_t)$ , which is introduced into Eq. (1) to give the foam strain rate as

$$\dot{\epsilon} = \left(\frac{a+1}{3a+1} \cdot \rho\right)^{-n} K \sigma^n \quad (19)$$

This equation converges to the original HD-c equation (Eq. (3)) as the strut aspect ratio  $a$  becomes large, i.e., when the node volume becomes negligible as compared to the strut volume. This new equation is labeled “modified Hodge–Dunand compression” (HD-c') in the following.

### 2.3.2. Compression mechanism with concentrated mass at nodes

For foams such as those created by the replication method, nodes exhibit larger cross-sections than struts, i.e., mass is concentrated at nodes. A highly simplified schematic for the new HD unit cell that exemplifies this geometry is shown in Fig. 4. Compared to the original HD unit cell of the same volume fraction with a uniform

size of strut and nodes, the cell with concentrated mass at node exhibits a larger solid volume responsible for sustaining the vertical compressive load. For the idealized geometry shown in Fig. 4, the ratio of the volume of vertical struts and node under compressive load ( $V_c$ ) to the total volume of solid ( $V_t$ ) in the unit cell of the foam structure is

$$\frac{V_c}{V_t} = \frac{2eb^2 + c^3}{6eb^2 + c^3} = \frac{2f^2 + g}{6f^2 + g} \quad (20)$$

where  $b$  is the strut width,  $c$  the node width and  $e$  the strut length (as shown in Fig. 4) and the parameters  $f$  and  $g$  are given as  $f = b/c$  and  $g = c/e$ ; these parameters can also be expressed as a function of the foam relative density and the node volume fraction  $V_n$ , as given in Appendix A. Assuming that the ratio of areas under compression scales with the ratio of volumes under compression, the creep rate of this system is estimated as

$$\dot{\epsilon} = K\sigma_v^n = K\sigma^n \left( \frac{2f^2 + g}{6f^2 + g} \cdot \rho \right)^{-n} \quad (21)$$

This equation is labeled “Hodge–Dunand concentrated mass” (HD-cm) in the following. The above assumption – taking an average strut/node cross-sectional area – does not fully describe the creep of the cell shown in Fig. 4 given the non-linear form of the creep law (Eq. (1)), but this geometry is in fact far from representative of replicated foams. Thus, refining the model further would necessitate specific information on the exact strut and node geometry, and would be more adequate for a finite-element model [21].

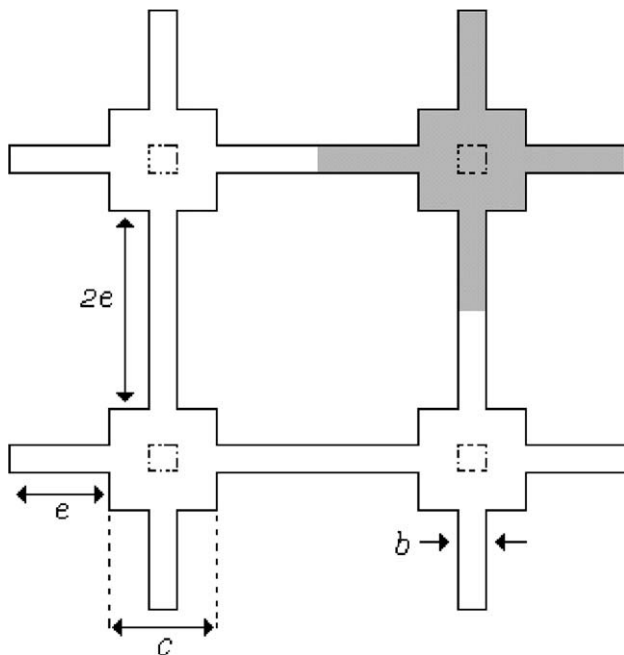


Fig. 4. Hodge–Dunand model ( $\rho = 0.05$ ) with mass concentration at nodes ( $V_n = 0.75$ ,  $f = b/c = 0.3$ , and  $g = c/e = 1.2$ ) showing unit cell (white) and repeat unit (shaded) with geometric parameters  $b$ ,  $c$ , and  $e$ .

#### 2.4. Summary of analytical creep models

The various analytical relationships for creep behaviors of metallic foams presented here are summarized in Table 1. All creep equations in Table 1 predict that the foam strain-rate sensitivities to stress (through the stress exponent  $n$ ) and temperature (through the activation energy  $Q$ , included in  $K = A \exp(-Q/RT)$ ) are equal to those of the monolithic material. However, the strain-rate sensitivity to the foam relative density varies among models. It is thus possible to normalize the strain rate of the foam by that of the monolithic material (Eq. (1)) to determine a factor, dependent on strut geometry (strut aspect ratio  $a$  and node parameters  $f$  and  $g$ ) and relative density  $\rho$ , expressing the increase in strain rate due to porosity at a given stress and temperature.

### 3. Experimental procedures

The nickel-base alloy J5 (Ni–22.5Mo–12.5Cr–1Ti–0.5Mn–0.1Al–0.1Y, in wt.%) was provided by the National Energy Technology Laboratory (Albany, OR). This alloy has a liquidus temperature of 1350 °C and was developed for solid-oxide fuel cell interconnects [22,23]. A J5 ingot was placed on top of a partially sintered preform of sodium aluminate space-holder powders (sieved to 355–500  $\mu\text{m}$ , purchased from Alfa Aesar) within a 20 mm-ID crucible, which was heated to 1450 °C under vacuum. Argon at 0.08 MPa pressure was then introduced in the furnace, which forced the melt into the evacuated pores of the preform. The solidified composite ingot was then machined into  $8 \times 4 \times 4 \text{ mm}^3$  specimens from which the space-holder was subsequently leached in an aqueous 10% HCl solution. The resulting foams were homogenized at 1100 °C for 4 h under argon, and annealed at 850 °C in air for 4 h, with water-quenching terminating each step. Monolithic J5 specimens were also machined and heat-treated similarly to the foams. Further processing details are given in Ref. [12].

Constant-load compression creep tests were performed in air at 850 °C in a creep frame with strain measured continuously by a linear voltage displacement transducer to an accuracy of  $\pm 2 \mu\text{m}$ . The secondary creep strain rate was determined from the slope of strain–time plots and each specimen was subjected to a series of increasing stresses in the range of  $\sim 10$ –100 MPa until accumulated strains of 0.1 and 0.3 had been reached in the foam and monolithic specimens, respectively.

### 4. Results

#### 4.1. Analytical results

Considering first the GA unit cell, the foam strain rate, after normalization by the strain rate of the monolithic material, is plotted in Fig. 5 for a typical creep exponent ( $n = 3$ ) as a function of relative density for the various

Table 1  
Existing and modified models for creep of foams.

Model name	Deformation mechanism	Strain-rate relationship	Equation
<i>Beam analysis – GA unit cell</i>			
GA-b	Gibson–Ashby bending	$\dot{\epsilon}_b = \frac{0.6}{n+2} \left( \frac{1.7(2n+1)}{n} \right)^n \rho^{-(3n+1)/2} K \sigma^n$	(2)
GA-b'	Modified Gibson–Ashby bending	$\dot{\epsilon}_{b'} = \frac{3.1}{n+2} \cdot \left( \frac{9.3 \cdot (2n+1)}{n} \right)^n \cdot \left[ \left( \frac{a-1}{2} \right)^{2+n} \cdot \left( \frac{a+1}{2} \right)^{2n-1} \right] \cdot K \sigma^n$	(9)
GA-s	Gibson–Ashby shear	$\dot{\epsilon}_{sh} = 1.8 \cdot 8.1^n \left[ \left( \frac{a-1}{2} \right) \cdot \left( \frac{a+1}{2} \right)^{2n-1} \right] \cdot K \sigma^n$	(12)
GA-bc	Gibson–Ashby bending/compression	$\dot{\epsilon}_{bc} = \dot{\epsilon}_{b'} + \left( \frac{3a+3}{9a+4} \cdot \rho \right)^{-n} \cdot K \sigma^n$	(16)
GA-sc	Gibson–Ashby shearing/compression	$\dot{\epsilon}_{sc} = \dot{\epsilon}_{sh} + \left( \frac{3a+3}{9a+4} \cdot \rho \right)^{-n} \cdot K \sigma^n$	(17)
<i>Beam analysis – HD unit cell</i>			
HD-c	Hodge–Dunand compression	$\dot{\epsilon}_c = \left( \frac{\rho}{3} \right)^{-n} \cdot K \sigma^n$	(3)
HD-c'	Modified Hodge–Dunand compression	$\dot{\epsilon}_{c'} = \left( \frac{a+1}{3a+1} \cdot \rho \right)^{-n} \cdot K \sigma^n$	(19)
HD-cm	Hodge–Dunand concentrated mass	$\dot{\epsilon}_{cm} = \left( \frac{2f^2+g}{6f^2+g} \cdot \rho \right)^{-n} \cdot K \sigma^n$	(21)
<i>Composite analysis</i>			
MF	Mean field	$\dot{\epsilon} = (A_E \rho^z)^{-(1+n)/2} \rho^{-(n-1)/2} K \sigma^n$	(4)

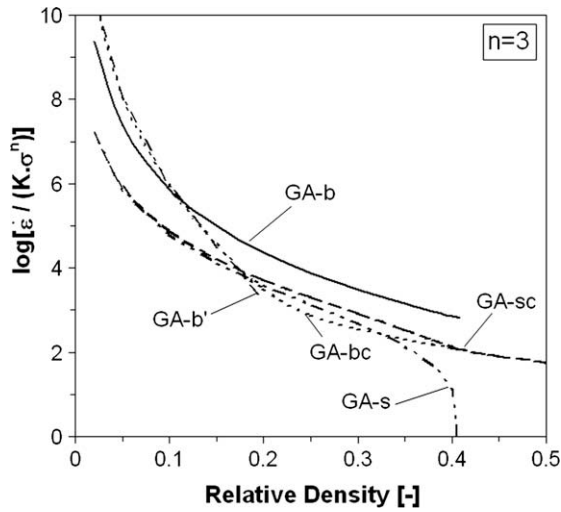


Fig. 5. Foam strain rate (normalized by that of the dense material with  $n = 3$ ) vs. foam relative density as calculated for various GA models. The GA-b model is not valid for  $\rho > 0.41$ .

GA models (GA-b, GA-b', GA-s, GA-bc and GA-sc). The modified GA-b' model (Eq. (9)) is close to the original GA-b model for low relative densities ( $\rho$  between 0.02 and 0.10) but predicts significantly lower strain rates for  $\rho \sim 0.15$ . Although the result of GA-b' presented in Fig. 5 are not exact due to approximations used in the derivation (Appendix B), this model is characterized by a more rapid decrease in foam strain rate as relative density increases. However, as the span of the struts become small, bending of struts becomes less and less important while shearing becomes controlling for the overall foam deformation (Fig. 3). Indeed, the GA-s shearing model (Eq. (12)), predicts faster creep rates than the GA-b or GA-b' model for  $\rho > 0.15$ . However, the GA-s model becomes invalid at a relative density  $\rho \sim 0.41$  for strut aspect ratio  $a = 1$  when the struts span  $d - t/2$  reaches zero. Above  $\rho \sim 0.41$ , all GA-b models are thus invalid and not plotted

in Fig. 5, despite in some cases showing positive values of strain rates.

Compressive deformation of the vertical struts is an additional mechanism which is added to the bending or shearing of the horizontal beams in models GA-bc (Eq. (16)) and GA-sc (Eq. (17)), respectively. Fig. 5 illustrates that the compressive contribution is negligible for relative density  $\rho < 0.20$ , where creep is governed by the fastest of the two simple mechanisms (modified bending for  $\rho < 0.15$  and shearing for  $0.15 < \rho < 0.20$ ). For  $\rho > 0.20$ , the compression term in Eq. (16) and Eq. (17) becomes dominant, so that the fastest of these two model controls the overall foam creep: the GA-sc model (compression and shearing) for  $0.20 < \rho < 0.41$ . However, the validity of these compression models becomes questionable for very high relative densities (say,  $\rho > 0.60$ ), where a composite model is more appropriate. Indeed, neither GA-bc nor GA-sc model predicts  $\log(\dot{\epsilon}/K\sigma^n) = 0$  for  $\rho = 1$ , as would be expected physically. In summary, for the GA unit cell, the fastest of the GA-b', GA-s, GA-bc and GA-sc models is expected to dominate creep deformation. For  $n = 3$ , it is the modified bending model (GA-b') for  $\rho < 0.15$  and shearing/compression (GA-sc) for  $\rho > 0.15$  (which gives the same result as bending/compression (GA-bc) for  $\rho > 0.41$ ).

Turning now to the HD unit cell, Fig. 6 shows the normalized foam strain rate as a function of relative density for the three HD models (HD-c, HD-c', and HD-cm) for a stress exponent  $n = 3$ . For comparison, the original GA-b model is also presented (but as pointed out earlier, is only valid for  $\rho < 0.41$ ). As already shown in Ref. [16], the HD-c model predicts much slower strain rates at low relative density than the GA-b model, but the two models converge for relative densities near  $\rho = 0.50$  (for  $n = 3$ ). Fig. 6 shows that the modified HD-c' model (Eq. (19)) diverges steadily from the original HD-c model as the relative density increases, with the mismatch reaching about

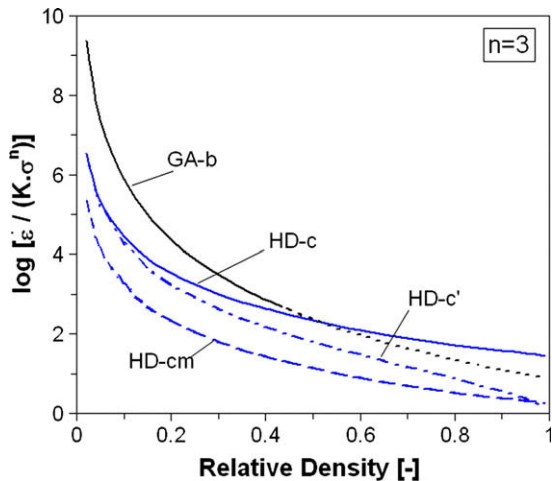


Fig. 6. Foam strain rate (normalized by that of the dense material with  $n = 3$ ) vs. foam relative density as calculated for various HD models. Also shown is the GA-b model, to help comparison with Fig. 5, which is however invalid for  $\rho > 0.41$ , where it is plotted as a dotted line.

one order of magnitude at full density  $\rho = 1$ , where the modified HD-c' model correctly predicts the creep response of the monolithic material (i.e.,  $\log(\dot{\epsilon}/K\sigma^n) = 0$ ). When concentrated mass at the node is considered (HD-cm model, Eq. (21)), the foam creep rate is further decreased as shown in Fig. 6. In this particular example,  $g = 18f^2$ , giving a node volume fraction of  $V_n = 0.75$  (Eq. (A5)) and a strut volume fraction of 0.25, as well as a ratio  $V_c/V_t = 0.83$  (from Eq. (20)).

#### 4.2. Experimental results

The replicated J5 foam specimens exhibited a density of  $4.0 \text{ g cm}^{-3}$ , corresponding to an open porosity of 54% ( $\rho = 0.46$ ). Fig. 7 shows the microstructure of the foam

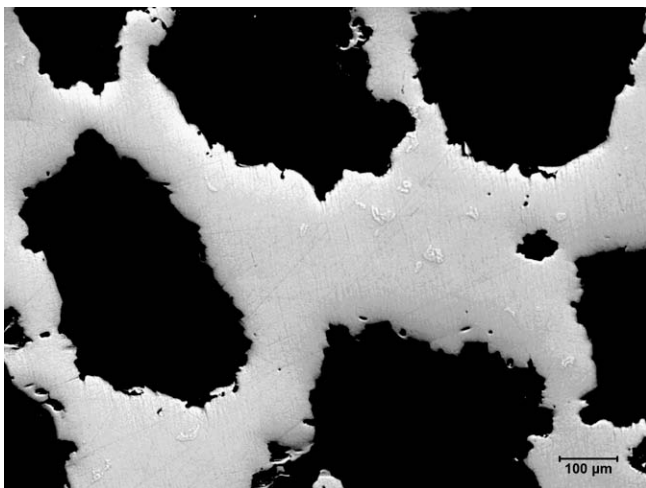


Fig. 7. Metallographic cross-section of open-cell J5 foam processed by casting replication of sodium aluminate performs. The foam exhibits a density of  $4.0 \text{ g cm}^{-3}$  corresponding to an open porosity of 54% ( $\rho = 0.46$ ).

which exhibits pore-free struts and nodes, unlike replicated foams produced by powder metallurgy [11]. There is thus no closed porosity. While it is difficult to ascertain from 2D micrographs whether the structure of this replicated foam is closer to the GA or the HD cells, concentrated mass at nodes is clearly observed in the structure, distinguishing the replicated foam structure from those of the idealized GA and HD cells with uniform struts.

Fig. 8 shows a rectangular J5 foam specimen employed in the creep experiment, along with examples of compressive strain–time plots obtained from the tests performed on foam specimens. Fig. 9 presents a double logarithmic plot of the strain rate vs. applied stress for J5 foams and monolithic J5 at  $850 \text{ }^\circ\text{C}$ . As anticipated, the solid J5 exhibited much lower strain rates than the J5 foams, at a given stress. Two creep regimes exist, each with a similar stress exponent for each material. At low strain rates ( $\dot{\epsilon} < 5 \times 10^{-8} \text{ s}^{-1}$ ), the stress exponent is low ( $n = 1.7$  and  $1.2$  for foam and monolith, respectively), while at high strain rates ( $\dot{\epsilon} > 5 \times 10^{-8} \text{ s}^{-1}$ ), it is high ( $n = 3.8$  and  $3.3$ , respectively). The average strain exponents of the materials are thus estimated as 1.5 and 3.5.

#### 5. Discussion

The various creep models developed in the present study are based on the two GA and HD unit cells (Figs. 1 and 2). While all of these newly derived models predict monotonically decreasing trend of creep rates with increasing foam relative density, the magnitude of the creep rate predicted by individual models varies widely. Generally, the mechanism (or combined mechanisms) predicting, at a given foam relative density, the fastest foam creep rate can be assumed to be dominant. These mechanisms are compared in the following discussion for three ranges of foam relative density (low, intermediate and high) and compared to experimental foam creep data.

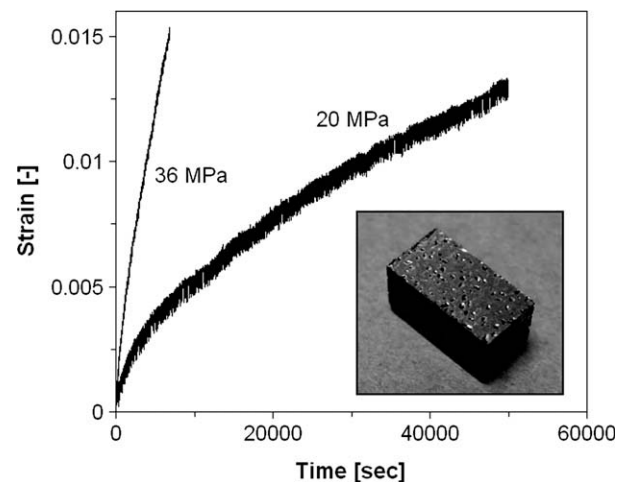


Fig. 8. Plot of strain vs. time for J5 foams subjected to compressive stresses of 20 and 36 MPa. Relative densities are 0.46 and 0.47, respectively. The inset presents an example of replicated J5 foam specimens ( $8 \times 4 \times 4 \text{ mm}^3$ ) used in creep testing.

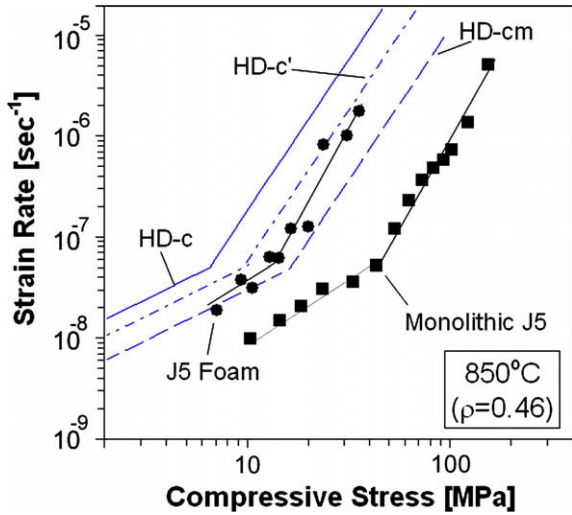


Fig. 9. Foam strain rate vs. applied stress as predicted by various HD models for  $\rho = 0.46$  and stress exponents  $n = 1$  and 3 (at low and high stress), using the experimental creep data for monolithic J5 for the creep constant  $K$  at 850 °C. Also shown are experimental creep data for the replicated J5 foam with  $\rho = 0.46$ , which are bracketed by predictions from the HD- $c'$  and HD-cm models (same parameters as in Fig. 4).

5.1. Low relative density ( $\rho < 0.20$ )

As shown in Fig. 10 for  $n = 4$ , the original GA-b model (Eq. (2)) and the composite MF model (Eq. (4)) have been reported to be in general agreement with experimental creep rates of aluminum foams with low relative density ( $\rho = 0.06\text{--}0.14$ ) [4,17]. This figure shows that, at low relative density, for the range  $0.05 < \rho < 0.15$ , the modified GA- $b'$  model predicts creep rates within a factor of 4 to the original GA-b model. Fig. 10 also shows that the GA- $b'$  model predicts higher creep rate than the GA-s model, for which strut bending is replaced by shearing,

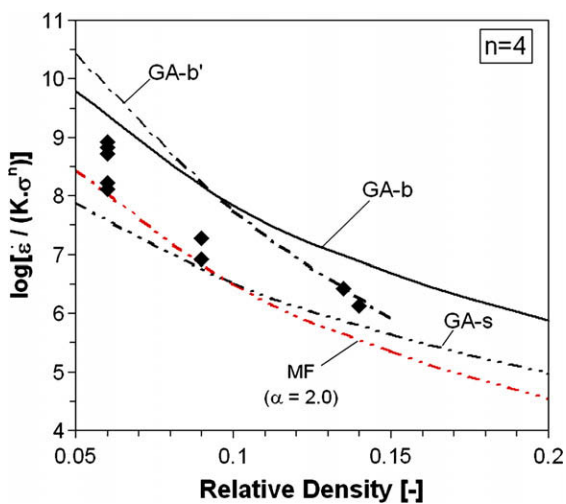


Fig. 10. Foam strain rate (normalized by that of the dense material with  $n = 4$ ) vs. foam relative density as calculated for the GA-b, GA- $b'$ , GA-s and MF models. Experimental data for Al foams measured in compression at 275 °C are also plotted [4].

indicating that the latter mechanism is not dominant for low relative densities. Considering the additional contribution provided by the compression of the vertical struts has a negligible effect at these low relative densities, i.e., the GA-bc and GA- $b'$  models overlap, as do the GA-sc and GA-s models (Figs. 5 and 10). The experimental creep data falls between the GA-s and the GA- $b'$  (or equivalently GA-b) models, which may indicate that the struts creep by a mixture of bending and shear, or more likely that they deform by one, the other or both mechanism in different locations of the foam, depending on their exact orientation with respect to the applied stress. The MF model also gives satisfactory agreement with the data. As expected, the strut compression models HD-c, HD- $c'$  and HD-cm models are not operative, and they all predict much lower strain rates than observed experimentally, i.e., by about two orders of magnitude as compared to the GA- $b'$  model.

5.2. Intermediate relative density ( $0.20 < \rho < 0.40$ )

In this range of relative density, the GA-s model which is governed by the shearing mechanism predicts higher strain rates than GA- $b'$ , and does not break down until  $\rho \sim 0.41$  (Fig. 5). When compression of vertical struts is considered to occur concurrently with shearing of the horizontal struts, resulting in the GA-sc model, the predicted creep rate is increased slightly. Furthermore, comparing the GA-s (or GA-sc) model with the GA-bc model with strut bending and compression, the latter model predicts slightly lower creep rates (Fig. 5). From these observations, it may be concluded that, at intermediate foam relative densities ( $0.20 < \rho < 0.40$ ), shearing has replaced bending as the controlling mechanism for creep of foams that exhibit GA-type structure. The range of densities where this is true varies with the value of the stress exponent ( $n = 3$  is used in Fig. 5).

Comparing Figs. 5 and 6, it is apparent that the two HD-c and HD- $c'$  models with cells deforming exclusively by strut compression predicts creep rates within a factor of two of those calculated with the GA-s, GA-sc and GA-bc models in the intermediate relative density range and for  $n = 3$ , despite very different cell architectures. Only when mass is concentrated at nodes are creep rates significantly slower (i.e., by a factor of seven when comparing models HD-cm and HD- $c'$  in Fig. 6 in the range  $0.20 < \rho < 0.40$ ), as expected from the increase of load-bearing mass within the cells.

5.3. High relative density ( $\rho > 0.40$ )

At high relative density, foams with the GA-type geometry creep solely by compression of their vertical struts with low aspect ratio. Specifically, as shown in Fig. 5, both the GA-bc and GA-sc model give near identical creep responses for  $\rho > 0.40$ , while the GA- $b'$  and GA-s models break down in this density range. Despite the difference in foam architectures, the HD- $c'$  model also predicts almost

exactly the same creep rate as the GA-bc and GA-sc models (Figs. 5 and 11). This is because in both cases, only vertical struts are deforming and both models have similar volume fraction of vertical struts.

In this regime of high relative densities, as for intermediate foam relative densities, the HD-cm model (with mass concentrated at nodes as typically exhibited by replicated foams) predicts lower strain rate than the HD-c' model. This, again, illustrates how the foam architecture can influence the creep response despite the fact that the deformation mode and relative density are unchanged. The composite MF model (Eq. (4)) with  $\alpha = 1.2$  is also presented in Fig. 11 and its predictions are close to those of the HD-cm model, despite very different approaches and assumptions.

Fig. 11 also compares the various creep model predictions with the experimental measurements for the J5 foams at high strain-rate regime ( $n = 3.5$ ). There is a reasonable fit with the HD-cm model, and also with the composite MF models (Eq. (4)), with  $\alpha$  between 1.2 and 2. The results therefore illustrate the significant influence of mass concentration at nodes in terms of improving foam creep resistance. Thus, despite the highly idealized nature of the above model, they seem to capture the essence of the creep behavior of replicated foams, which exhibit relatively high porosity with irregular node structures.

In closing, we note that while the analytical models developed here are discussed in the context of metallic foams, they are equally applicable to other creeping porous materials, including polymer and ceramic foams.

## 6. Conclusions

Analytical models for the creep of cellular materials based on engineering beam analysis have been derived for various possible deformation mechanisms and strut archi-

tures, based on two cell architectures previously studied by Gibson and Ashby and by Hodge and Dunand, respectively. Some important assumptions postulated by the original models, including negligible mass at nodes, have been relaxed, so that the models developed here are more accurate and valid up to higher relative density values.

For a typical stress exponent  $n \sim 3$ , bending of struts is found to control the creep response for foams with low relative density (up to  $\sim 0.20$ ), while shearing is the dominant mechanism for relative densities between  $\sim 0.20$  and  $\sim 0.40$ . The GA-b' and GA-s models may be used to predict the creep of foams in these two relative density regimes, respectively. When relative density exceeds  $\sim 0.40$ , compressive creep of strut is dominant, and the GA-sc, GA-bc, and HD-c' models equivalently describe the creep behavior. For these high relative density foams, non-uniform strut cross-section and mass concentration at nodes may occur, and these can further decrease the foam creep rate, as described in the HD-cm model which is in agreement with experimental result on Ni-base replicated foams.

## Acknowledgements

The authors acknowledge Dr. P.D. Jablonski (NETL) for supplying the J5 alloy, and Dr. R. Bhat (GE Global Research Center), Dr. J.D. DeFouw, and J.A. Scott (Northwestern University) for useful discussions. This research was supported by NASA through a subcontract from the General Electric Company (award NNC06CB31C). Y.B. also acknowledges Chulalongkorn University for the Grant for Development of New Faculty Staff (1/2008).

## Appendix A

### A.1. Determining $a(\rho)$ for the GA cell

The relative density  $\rho$  of the GA cell shown in Fig. 1 can be calculated by considering the volume fractions of struts and nodes as

$$\rho = \frac{\frac{9}{2}t^2d + t^3}{(2d + t)^3} \quad (\text{A1})$$

where  $d$  is the strut half length and  $t$  is the strut (or node) thickness, as shown in Fig. 1. This equation can be rewritten solely as a function of the strut aspect ratio  $a = 2d/t$  as

$$\rho = \frac{\frac{9}{4}a + 1}{a^3 + 3a^2 + 3a + 1} \quad (\text{A2})$$

Solving the resulting cubic equation for the aspect ratio  $a$  gives

$$a = \frac{1}{2\rho} \cdot m^{1/3} + \frac{3}{2m^{1/3}} - 1 \quad (\text{A3})$$

where the parameter  $m$  is

$$m = \left(-5 + \sqrt{(25 - 27/\rho)}\right) \cdot \rho^2 \quad (\text{A4})$$

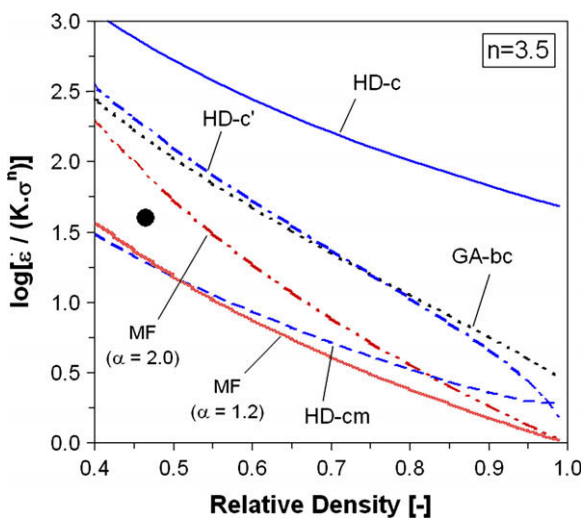


Fig. 11. Foam creep rate (normalized by that of the dense material with  $n = 3.5$ ) vs. foam relative density as calculated for the GA-bc, HD-c, HD-c', HD-cm, and MF models. Also shown is experimental data for J5 foam (for  $n \sim 3.5$ ).

A.2. Determining  $f(\rho, V_n)$  and  $g(f, V_n)$  for the HD model

The parameters  $f$  and  $g$  are defined as ratios  $f = b/c$  and  $g = ce$ , where the dimensions  $b$ ,  $c$ , and  $e$  are given in Fig. 4. A relationship between  $f$  and  $g$  is found by considering the volume fraction of nodes,  $V_n$ :

$$V_n = \frac{c^3}{c^3 + 6b^2e} = \frac{1}{\left(1 + \frac{6f^2}{g}\right)} \quad (\text{A5})$$

Then, the parameter  $g$  can be expressed as

$$g = \frac{6f^2}{\left(\frac{1}{V_n} - 1\right)} \quad (\text{A6})$$

The values of  $f$  and  $g$  are also related through the volume fraction of a HD-cm unit cell as

$$\rho = \frac{6eb^2 + c^3}{(c + 2e)^3} \quad (\text{A7})$$

This equation can be rewritten as a function of the ratios  $f$  and  $g$  as

$$\rho = \frac{6f^2g^2 + g^3}{8 + 12g + 6g^2 + g^3} \quad (\text{A8})$$

The parameters  $f$  and  $g$ , for a given foam relative density  $\rho$  and node volume fraction  $V_n$ , are determined by solving the cubic equation (A8) and using the relationship in Eq. (A6). This gives

$$f = \left( \frac{(V_n - 1)((\rho^2 V_n^2)^{1/3} + \rho V_n((\rho^2 V_n^2)^{-1/3} + 1))}{3V_n(\rho V_n - 1)} \right)^{1/2} \quad (\text{A9})$$

$$g = \frac{6V_n((\rho^2 V_n^2)^{1/3} + \rho V_n((\rho^2 V_n^2)^{-1/3} + 1))}{(1 - \rho V_n)} \quad (\text{A10})$$

Appendix B

To determine the values of the constants  $k_1$  and  $k_2$  in Eq. (8), we first consider the limit of  $n \rightarrow \infty$  and use the yield stress  $\sigma_y$  for  $\sigma_s$ . This gives

$$1 = 2k_2 \cdot \left(\frac{a-1}{2}\right) \cdot \left(\frac{a+1}{2}\right)^2 \cdot \frac{\sigma}{\sigma_y} \quad (\text{B1})$$

Next, we find a relationship between the term  $\left[\left(\frac{a-1}{2}\right) \cdot \left(\frac{a+1}{2}\right)^2\right]^{-1}$  and the relative strength  $\frac{\sigma}{\sigma_y}$ , based on the semi-empirical strength–density relationship proposed by Gibson and Ashby [1]:

$$\frac{\sigma}{\sigma_y} \approx 0.3\rho^{3/2} \quad (\text{B2})$$

Fig. B1 shows the monotonically increasing relationship of the  $a$ -containing term with respect to the relative strength, with the individual data points calculated from a set of equally spaced relative density values between 0 and 0.15. To estimate the relation between the two parameter sets,

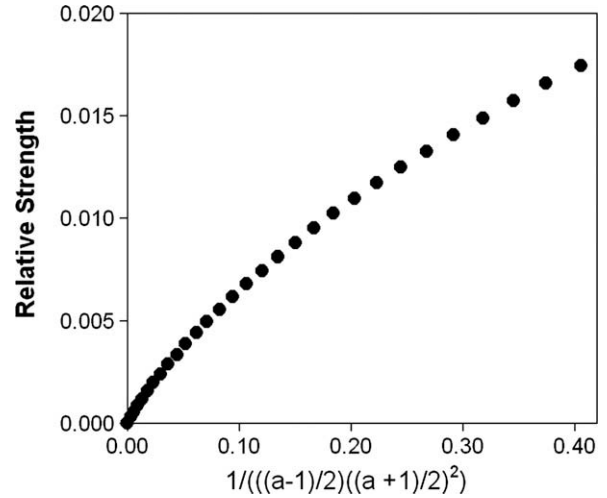


Fig. B1. Plot of relative strength  $\frac{\sigma}{\sigma_y}$  (calculated from Eq. (B2)) and the factor  $\left[\left(\frac{a-1}{2}\right) \cdot \left(\frac{a+1}{2}\right)^2\right]^{-1}$  (calculated from Eq. (A3)) for a set of equally spaced relative density values between 0 and 0.15. A near linear relationship exists, with an average proportionality factor of 0.054 leading to Eq. (B3).

a slope of any two adjacent data points in Fig. B1 is calculated and the average slope is determined. From this, we obtain

$$\frac{\sigma}{\sigma_y} \approx \frac{0.054}{\left(\frac{a-1}{2}\right) \cdot \left(\frac{a+1}{2}\right)^2} \quad (\text{B3})$$

From Eqs. (B1) and (B3),  $k_2$  is thus determined to be 9.3.

Similarly,  $k_1$  is determined by considering Eq. (8) at the other limit,  $n = 1$ , with  $\sigma/\varepsilon$  being replaced by  $E$ , the foam Young’s modulus, and  $\sigma_s/\varepsilon_s$  replaced by  $E_s$ , the monolithic Young’s modulus. The equation reduces to

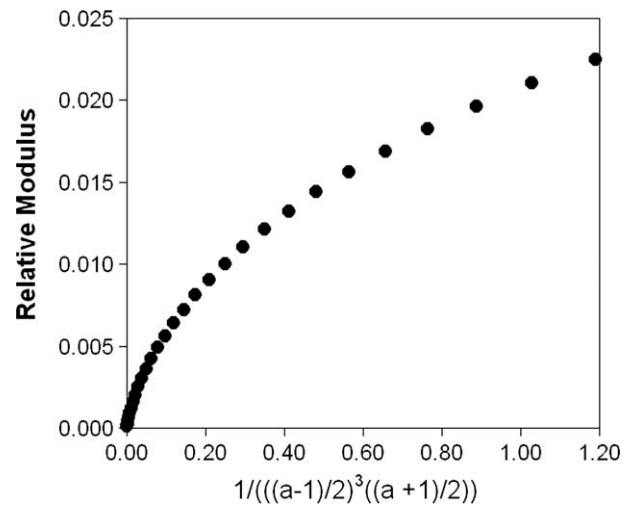


Fig. B2. Plot of relative modulus  $\frac{E}{E_s}$  (given by Eq. (B5)) and the factor  $\left[\left(\frac{a-1}{2}\right)^3 \cdot \left(\frac{a+1}{2}\right)\right]^{-1}$  (calculated from Eq. (A3)) for a set of equally spaced relative density values between 0 and 0.15. The average proportionality factor is 0.035 leading to Eq. (B6).

$$\frac{E_s}{E} = k_1 k_2 \left(\frac{a-1}{2}\right)^3 \cdot \left(\frac{a+1}{2}\right) \quad (\text{B4})$$

We then find a relationship between the term  $\left[\left(\frac{a-1}{2}\right)^3 \cdot \left(\frac{a+1}{2}\right)\right]^{-1}$  and  $\frac{E}{E_s}$ , based on the semi-empirical modulus–density relationship suggested by Gibson and Ashby [1]:

$$\frac{E}{E_s} \approx \rho^2 \quad (\text{B5})$$

Fig. B2 shows how the relative modulus relates to the  $a$ -containing term in Eq. (B4). A similar procedure as used above for relative strength is employed, and this results in a relation between the relative modulus and the second  $a$ -containing term given by

$$\frac{E}{E_s} \approx \frac{0.035}{\left(\frac{a-1}{2}\right)^3 \cdot \left(\frac{a+1}{2}\right)} \quad (\text{B6})$$

Introducing Eq. (B6) into Eq. (B4), it follows that  $k_1 = 3.1$ .

## References

- [1] Gibson LJ, Ashby MF. Cellular solids. Cambridge, UK: Cambridge University Press; 1997.
- [2] Banhart J. Prog Mater Sci 2001;46:559.
- [3] Korner C, Singer RF. Adv Eng Mater 2000;2:159.
- [4] Andrews EW, Gibson LJ, Ashby MF. Acta Mater 1999;47:2853.
- [5] Andrews EW, Huang JS, Gibson LJ. Acta Mater 1999;47:2927.
- [6] Andrews EW. Mater Lett 2006;60:618.
- [7] Quadbeck P, Kaschta J, Singer RF. Adv Eng Mater 2004;6:635.
- [8] Bram M, Stiller C, Buchkremer HP, Stover D, Baur H. Adv Eng Mater 2000;2:196.
- [9] Esen Z, Bor S. Scr Mater 2007;56:341.
- [10] Brothers AH, Scheunemann R, DeFouw JD, Dunand DC. Scr Mater 2005;52:335.
- [11] Bansiddhi A, Dunand DC. Intermetallics 2007;15:1612.
- [12] Boonyongmaneerat Y, Dunand DC. Adv Eng Mater 2008;10:379.
- [13] Despois JF, Marmottant A, Salvo L, Mortensen A. Mater Sci Eng A 2007;462:68.
- [14] Marchi CS, Mortensen A. Acta Mater 2001;49:3959.
- [15] Zhao YY, Sun DX. Scr Mater 2001;44:105.
- [16] Hodge AM, Dunand DC. Metall Mater Trans A 2003;34:2353.
- [17] Mueller R, Soubielle S, Goodall R, Diologent F, Mortensen A. Scr Mater 2007;57:33.
- [18] Hakamada M, Asao Y, Kuromura T, Chen Y, Kusuda H, Mabuchi M. Acta Mater 2007;55:2291.
- [19] German RM. Sintering theory and practice. New York (NY): John Wiley & Sons, Inc.; 1996.
- [20] Frost HJ, Ashby MF. Deformation-mechanism maps: the plasticity and creep of metals and ceramics. Oxford: Pergamon Press; 1982.
- [21] Oppenheimer SM, Dunand DC. Acta Mater 2007;55:3825.
- [22] Jablonski PD, Alman DE. Int J Hydrogen Energy 2007;32:3705.
- [23] Geng SJ, Zhu JH, Lu ZG. Scr Mater 2006;55:239.